Brief Report

DOI: 10.5582/bst.2022.01256

Real-time intraoperative near-infrared autofluorescence imaging to locate the parathyroid glands: A preliminary report

Bei Qian[§], Ximeng Zhang[§], Kaijian Bing, Longqing Hu, Xincai Qu, Tao Huang, Wei Shi[*], Shoupeng Zhang[*]

Department of Thyroid and Breast Surgery, Union Hospital, Tongji Medical College, Huazhong University of Science and Technology, Wuhan, Hubei, China.

SUMMARY Identification and localization of parathyroid glands (PGs) remains a challenge for surgeons. The aim of this study was to evaluate the efficiency of intraoperative near-infrared autofluorescence (NIRAF) imaging to detect PGs in thyroid and parathyroid diseases. Seventy-six patients undergoing surgery for thyroid or parathyroid diseases between July 9, 2020 and August 20, 2021 were retrospectively analyzed. Intraoperative carbon nanoparticle (CN) negative imaging and handheld NIRAF imaging were successively performed for each patient. Of 206 PGs that needed to be identified for surgery, 162 were identified by NIRAF imaging, with a theoretical rate of identification of 78.64%. This was higher than the rate of identification with CN negative imaging, which was 75.73%. The number of PGs identified by NIRAF imaging and CN negative imaging did not differ significantly in either total thyroidectomy or thyroid lobectomy. In addition, the autofluorescence (AF) intensity of secondary parathyroid adenoma was weaker than that of normal PGs. NIRAF imaging is potentially a more efficient tool for identification of PGs than CN negative imaging, with a shorter learning curve and lower risk. It may not be well-suited to secondary hyperthyroidism or adenoma, but it was more efficient at identifying excised specimens than visual identification by a surgeon.

Keywords parathyroid glands (PGs), near-infrared autofluorescence (NIRAF) imaging, carbon nanoparticles (CNs), identification, localization.

1. Introduction

With the increasing incidence of thyroid cancer (THCA) worldwide, thyroidectomy has become one of the most common endocrine surgeries (*1*). However, hypoparathyroidism caused by surgical injury remains a challenge for surgeons. The reported incidence of permanent hypoparathyroidism after total thyroidectomy is 0.5-6.6% and that of temporary hypoparathyroidism after thyroid surgery is 6.9-46% (*2,3*). Moreover, the risk of iatrogenic injury and inadvertent removal of parathyroid glands (PGs) increases with the extent of dissection or the complexity of the surgery (*4*). Tufano *et al*. reported that the incidence of permanent hypoparathyroidism following reoperative central compartment neck dissection can reach 9.5% (*5*).

Currently, conventional measures to reduce the risk of postoperative hypoparathyroidism mainly rely on visual recognition by a surgeon and preservation of PGs and their vascular pedicles, which are highly dependent on the surgeon's experience (*6*). However, PGs are very small and similar in color to adipose or connective tissue and even lymph nodes (LNs), and they are usually embedded within the surrounding tissue or behind the thyroid gland, so even experienced surgeons can unintentionally remove them at a rate as high as 9.1-15% (*1,7*). For surgeons with less experience or beginners in thyroid surgery, the incidence will be higher. Intraoperative frozen biopsy is the "gold standard" to confirm that the specimen removed is indeed a PG, but it involves considerable time and cost and may cause damage to the blood supply of PGs (*8*). Early studies suggested that injections of fluorescent agents such as methylene blue or indocyanine green (ICG) could aid in the intraoperative detection of PGs, but they have not been widely adopted (*9*). Moreover, these exogenous fluorophores were considered likely to lead to adverse reactions to the dye or injection (*10*).

In 2011, Paras *et al*. first reported that PGs emit autofluorescence (AF) when stimulated with a 785-nm wavelength laser (*11*). The fluorescence intensity of PGs is reported to be much greater than that of the

thyroid and all other surrounding tissue, with peak fluorescence occurring at 820 to 830 nm (*11*). Moreover, this technique does not rely on any exogenous drugs and dyes, thus avoiding possible adverse reactions. Since then, intraoperative near-infrared autofluorescence (NIRAF) imaging has been increasingly used to detect PGs. In addition, carbon nanoparticles (CNs) with an average diameter of 150 nm have also been found to be useful in identifying PGs, thanks to their high degree of lymphatic system tropism, tracing speed, rate of dyeing black, and a high color contrast with the surrounding tissue (*12*). However, the available data to evaluate and compare the effectiveness of the two methods in identifying PGs are still insufficient. The aim of the present study was to compare NIRAF imaging and CN negative imaging to evaluate the efficiency of NIRAF imaging in detecting PGs in thyroid and parathyroid diseases.

2. Patients and Methods

2.1. Study design

Subjects were 76 patients seen at the Thyroid and Breast Disease Center at Wuhan Union Hospital between July 9, 2020 and August 20, 2021. The inclusion criteria were: (1) age > 18 years; (2) no serious systemic disease; (3) patients underwent surgery; and (4) informed consent was provided. Patients who met any of the following criteria were excluded: (1) missing baseline information; (2) age ≤ 18 years; (3) having a severe systemic disease; or (4) lateral cervical LN metastasis. The data collected in this study included: patient ID, gender, age, the number of PGs that were detected by the two methods, the procedure undergone, and the postoperative histopathological diagnosis. Surgical procedures included total thyroidectomy with bilateral central lymph node dissection (CLND) and unilateral thyroid lobectomy with CLND or parathyroidectomy. Intraoperative CN negative imaging and handheld NIRAF imaging was successively performed for each patient.

2.2. Operative and imaging procedures

All of the surgeries were performed independently by two experienced thyroid surgeons. For the thyroid surgery, an incision parallel to a horizontal skin crease was made. The skin, subcutaneous tissue, adipose tissue, and platysma muscle were successively incised. A skin flap down to the superficial surface of the sternohyoid muscle was dissected upward to the thyroid cartilage and downward to the sternal notches, with the anterior jugular veins left in place (*13*). The midline raphe was identified and incised, and the sternohyoid and sternothyroid muscles were pulled laterally until the thyroid capsule was clearly identified. Care should be taken to keep the fibrous capsule of the thyroid gland intact, otherwise the injected CNs may leak out, contaminate the surgical field, and even cause infection. The lower third of the thyroid gland was exposed and 0.1 mL of CNs (in the form of an injected suspension at a concentration of about 50 mg per ml) were injected into the gland with a fine needle to a depth of about one third of the gland. Excessively dissected glands may cause damage to the surrounding lymphatic network, affecting the action of CNs after injection (*12*). The injected gland was gently massaged with gauze for about 1 minute and the surgeon waited for the gland to completely blacken. The thyroid gland was then mobilized to expose the central neck area. PGs were carefully identified by negative visualization while the LNs and thyroid gland were stained black, indicating positive visualization, and photographed intraoperatively. The operating room lights were subsequently turned off, and an infrared camera probe (Micro-intelligence Technology, Hunan, China) encapsulated in a sterile envelope was placed 20 cm away from the surgical field for near-infrared fluorescence imaging (NIFI) to detect the possible location of PGs (Figure 1). The numbers of PGs detected by the two approaches were recorded separately. The thyroid gland was subsequently removed and a rapid intraoperative pathological examination was performed. Based on the pathology results, the decision was made whether to perform a preventive CLND. For parathyroid surgery, thyroid exposure was achieved as described above. PGs were successively imaged with CN negative imaging and NIRAF imaging as described above. The diseased PGs were then removed and sent for a rapid intraoperative pathological examination.

2.3. Statistical analysis

Continuous variables with a normal distribution were expressed as the mean ± standard deviation (SD) or as the median and interquartile range (IQR). Categorical variables were expressed in terms of frequency and

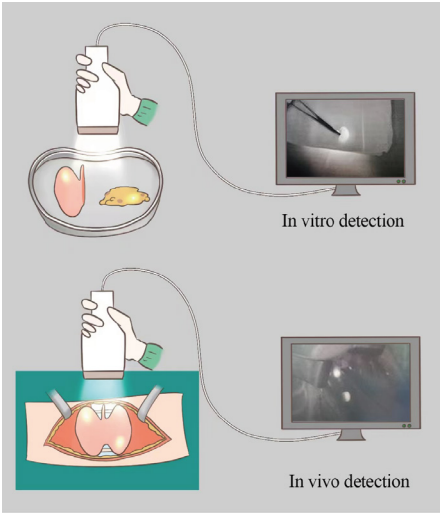

Figure 1. Diagram of NIRAF detection of parathyroid glands *in vivo* and *in vitro*.

percentages. A chi-square test was used to analyze categorical variables, while a *t*-test was used to compare continuous variables. Statistical significance was a two-sided $P < 0.05$. All statistical analyses were performed using R Studio version 4.0.3 (*http://www.r-project.org*).

2.4. Ethical approval and informed consent

The study was conducted in accordance with the ethical standards of the Declaration of Helsinki as well as national and international guidelines and approved by the Ethical Committee of the Union Hospital, Tongji Medical College of Huazhong University of Science and Technology (0304-01). Written consent for publication of patient data was obtained from the patients themselves.

3. Results and Discussion

3.1. Demographic characteristics and clinical features

During the period between July 9, 2020 and August 20, 2021, a total of 76 patients were identified and included in the present study. Table 1 summarizes the clinicopathological characteristics and treatment information of the patients. The mean age of all patients was 41.5 years (IQR: 32.8-50.5, range: 22-63). Twenty-seven patients (35.5%) were male and 49 (64.5%) were female. The final histopathological diagnosis for patients was THCA in 66 (86.8%), benign nodular goiter in 9 (11.8%) and parathyroid adenoma in 1 (1.3%). Of all patients, 25 (32.9%) underwent a total thyroidectomy plus CLND, 3 (3.9%) underwent a total thyroidectomy, 41 (53.9%) underwent a thyroid lobectomy plus CLND, 6 (7.9%) underwent a thyroid lobectomy, and 1 (1.3%) underwent a parathyroidectomy.

3.2. Rate of identification of PGs by the two approaches

According to the theoretical calculation of four PGs per patient, a total of 206 PGs (this number was calculated by procedure) were potentially identifiable in this study. However, 162 PGs were identified by NIRAF imaging, with a theoretical rate of identification of 78.64%. CN negative imaging identified 156 PGs, with a rate of 75.73%. Intraoperative images are shown in Figure 2. NIRAF imaging had a higher rate of identification than CN negative imaging, although the difference was not significant ($P = 0.481$). For total thyroidectomy, NIRAF imaging identified 3.2 PGs on average, while CN negative imaging identified 3.0 PGs. There were no significant differences in the number of PGs identified ($P = 0.457$). For thyroid lobectomy, an average of 1.6 PGs were identified by NIRAF imaging and 1.5 PGs were identified by CN negative imaging. There were no significant differences in the number of PGs identified (P=0.843). Table 2 shows the results of a statistical analysis. Interestingly, the AF intensity of a secondary parathyroid adenoma was weaker than that of a normal PG (Figure 3).

3.3. Discussion

To the extent known, this is the first study to provide data on evaluating the feasibility and efficiency of NIRAF imaging to detect PGs in real time during thyroid and parathyroid surgeries by comparing that modality to CN negative imaging. Results indicated that both NIRAF imaging and CN negative imaging identified PGs at an acceptable rate. The rate of PG identification did not differ significantly between NIRAF imaging and CN negative imaging in either total thyroidectomy or thyroid lobectomy, but NIRAF imaging was considered to have greater clinical value and potential for widespread use because of its convenience, safety, and reproducibility. Because of its simplicity and speed, NIRAF imaging had a shorter learning curve for beginners and less

Table 1. Demographics and clinicopathological characteristics of all patients

Parameters	All patients ($n = 76$)
Age, years (median [IQR])	41.5 (IQR: 32.8-50.5)
Gender, *n* (%)	
Male	27 (35.5%)
Female	49 (64.5%)
Histopathological diagnosis	
Thyroid cancer	66 (86.8%)
Benign nodular goiter	9 (11.8%)
Parathyroid adenoma	1 (1.3%)
Procedure, *n* (%)	
Total thyroidectomy plus CLND	25 (32.9%)
Total thyroidectomy	3 (3.9%)
Thyroid lobectomy plus CLND	41 (53.9%)
Thyroid lobectomy	6 (7.9%)
Parathyroidectomy	1 (1.3%)

IQR: interquartile range; CLND: central lymph node dissection.

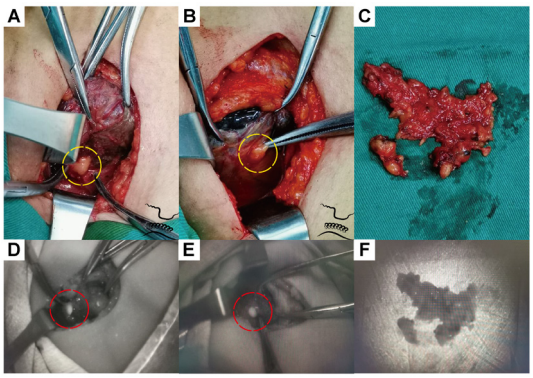

Figure 2. NIRAF imaging and CN negative imaging of the parathyroid glands during a thyroidectomy; the parathyroid glands are circled in red or yellow. (A) CN negative imaging of the upper right parathyroid gland; **(B)** CN negative imaging of the lower right parathyroid gland; **(C)** Visible light images of the isolated right central lymph node specimen; **(D)** NIRAF imaging of the upper right parathyroid gland; **(E)** NIRAF imaging of the lower right parathyroid gland; **(F)** NIRAF imaging of the isolated right central lymph node specimen.

Table 2. Accuracy of identification of 206 parathyroid glands by NIRAF imaging and CN negative imaging

Parameters	NIRAF	CN negative imaging	*P* value
Number identified/total	162/206	156/206	-
Rate of identification	78.64%	75.73%	0.481
Mean number identified for total thyroidectomy	3.19	3.00	0.457
Mean number identified for thyroid lobectomy	1.55	1.53	0.843

NIRAF: near-infrared autofluorescence imaging; CNs: carbon nanoparticles.

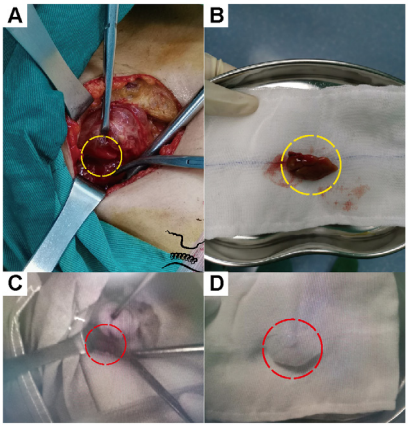

Figure 3. NIRAF imaging and CN negative imaging of a parathyroid adenoma during a parathyroidectomy; the parathyroid glands are circled in red or yellow. (A) CN negative imaging of an upper right parathyroid adenoma; **(B)** Visible light images of the isolated upper right parathyroid adenoma; **(C)** NIRAF imaging of the upper right parathyroid adenoma; **(D)** NIRAF imaging of the isolated upper right parathyroid adenoma.

experienced thyroid surgeons. Moreover, there was no need to use any exogenous dyes or colorant, so NIRAF imaging posed a lower risk during surgery. In addition, the AF intensity of a secondary parathyroid adenoma was weaker than that of a normal PG. The AF intensity did not differ significantly compared to that of the surrounding tissue in the central neck.

The identification and location of PGs is a well-known challenge of thyroid or parathyroid surgery (*14*). Accidental injury or resection may lead to hypoparathyroidism, which means temporary or permanent hypocalcemia and other accompanying symptoms (*15*). Many early intraoperative methods of identifying PGs have been reported, such as intravenous injection of methylene blue(*10*) or ICG (*16*) or 99m-Technetium sestamibi (MIBI) (*17*), CN negative imaging (*18*), measurement of parathyroid hormone levels from needle aspirates of tissue specimens (*19*) and aspartate aminotransferase to lactate dehydrogenase ratios from suspended tissue specimens (*20*). However, few of these methods have been widely adopted and promoted in clinical practice (*21*). Although a frozen section was the gold standard to confirm that a specimen was a PG, obtaining it could damage the integrity of PGs and involve considerable time and cost (*8*). However, the discovery of the intrinsic fluorescence of PGs at NIR wavelengths has allowed the identification of PGs in real time during surgery. Although the detailed mechanism of AF is not yet clear, the mainstream view is that AF was derived from the calcium-sensing receptor protein, which was most concentrated in the chief cells of PGs, less concentrated in the thyroid, and not present in other tissues of the neck (*22*). In patients with secondary hyperparathyroidism, the down-regulation of calcium-sensing receptors leads to a decrease in fluorescence intensity compared to that of normal PGs (*23*). In addition, Squires *et al*. noted significantly lower quantified absolute values of parathyroid AF in situ and ex vivo and significantly lower parathyroid-to-background AF ratios for patients with *vs*. without multiple endocrine neoplasia type 1 (MEN1) (*24*).

In the present study, 78.64% of PGs were detected with NIRAF imaging prior to the dissection, which was consistent with previous reports (*25*). This is because AF was difficult to detect when PGs were buried in surrounding tissue of a certain thickness. Early studies confirmed that about 77-100% of PGs were detectable by NIRAF imaging (*6*). Moreover, Benmiloud *et al*. studied parathyroid AF in 93 patients and found that 68% PGs were identified via NIRAF imaging before they were visualized by the surgeon (*26*). A definite advantage of NIRAF imaging is that it can detect PGs in excised specimens more quickly and efficiently than visual identification by a surgeon (Figure 1). This contention was corroborated by Takahashi *et al*., who emphasized that the sensitivity of NIRAF imaging (82.9%) at detecting PGs from thyroidectomy specimens was significantly higher than that of visual inspection by a surgeon (61.0%) (*27*). NIRAF imaging did not significantly improve the rate of parathyroid identification compared to CN negative imaging (78.64% *vs*. 75.73%), but the former is preferred by surgeons because it has a shorter learning curve and involves lower risk. Different studies have reached conflicting conclusions regarding postoperative hypoparathyroidism or hypocalcemia. A multicenter randomized clinical trial involving 241 patients found that NIRAF-assisted thyroidectomy significantly decreased the rate of early postoperative hypocalcemia compared to a conventional thyroidectomy (9.1% *vs*. 21.7%) with no significant differences in the rate of permanent hypocalcemia (0% *vs*. 1.6%) (*28*). However, Papavramidis *et al*. concluded that the use or lack of NIRAF imaging had no effect on temporary postoperative hypoparathyroidism or hypocalcemia, while NIRAF could drastically

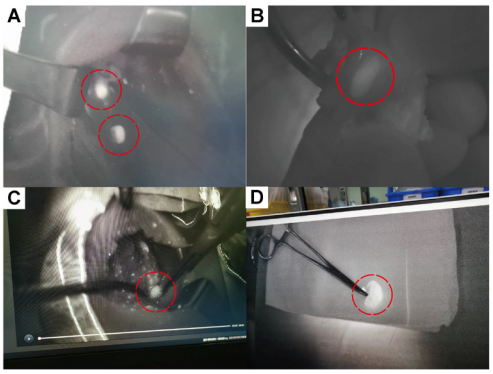

Figure 4. NIRAF imaging of the parathyroid glands under different conditions; the parathyroid glands are circled in red. (A) Ipsilateral upper and lower parathyroid glands in the surgical field; **(B)** A parathyroid gland embedded in an isolated lymph node specimen; **(C)** A parathyroid gland embedded in the thymus; **(D)** A single normal parathyroid gland placed on gauze.

decrease the incidence of permanent postoperative hypoparathyroidism or hypocalcemia (*6*).

Although the fluorescence intensity in this study was not quantified to distinguish PGs from surrounding tissues as in previous studies, PGs emitted significantly stronger fluorescence than surrounding tissues (Figures 2 and 4). Kin *et al*. found that the average fluorescence intensity of PGs calculated by the software Image J was 1.95-5.2 times that of surrounding tissues (*1*). However, McWade *et al*. reported emission intensity from PGs 2.4-8.5 times higher than that from surrounding tissue (*29*). Berber *et al*. found that the optimal tissue/background AF intensity thresholds to predict PGs ranged between 1.46 and 1.72 for different backgrounds (*8*). Moreover, the fluorescence ratio of PGs to surrounding tissues increased with an increase in PG volume and weight (*30*). Even an hour after excision or formalin fixation, the AF of PGs remained stable (*22*). The equipment was set up before surgery and intraoperative imaging took only 2-3 minutes, so the total operating time was not delayed.

However, as a tool for intraoperative real-time identification and localization of PGs, NIRAF imaging still has the following deficiencies: (1) when NIRAF imaging detection equipment was in operation, the ambient light in the operating room had to be completely turned off to eliminate the interference of white light as much as possible; (2) Due to the weak penetration of near-infrared rays, AF may be difficult to detect when the surface tissue of the PG covers more than several millimeters; (3) NIRAF imaging could not evaluate the activity and blood perfusion status of PGs and thus failed to provide guidance for timely intraoperative autologous transplantation or in-situ preservation; (4) Patients with secondary hyperparathyroidism or parathyroid adenoma may exhibit lower intrinsic AF than those with primary hyperparathyroidism or normal PGs; and (5) The equipment needs to be more compact and easier to operate to facilitate real-time intraoperative use. In summary, NIRAF imaging cannot completely replace frozen sections in the short term, but the former could be used as a complement to visual recognition by a surgeon and to minimize unnecessary frozen biopsies in some cases. The above limitations would also provide a direction for the future development and improvement of this technology.

There were certain limitations that should be acknowledged. Firstly, the findings were limited by the insufficient sample size and single-institution nature of this study. Prospective multicenter randomized controlled studies with large sample sizes need to be conducted to further confirm the current results. Secondly, more postoperative indicators such as short- and long-term parathyroidism and serum calcium levels need to be included to better evaluate the effectiveness of NIRAF imaging in preventing hypoparathyroidism. Thirdly, although AF could distinguish PGs from non-PG tissue, histopathological verification may be necessary to confirm that certain samples were indeed PGs.

In conclusion, NIRAF imaging is a potentially more efficient tool for identification of PGs than CN negative imaging, with a shorter learning curve and lower risk. It may not be well-suited to secondary hyperthyroidism or adenoma, but it is more efficient at identifying excised specimens than visual identification by a surgeon.

Acknowledgements

The authors would like to thank all of the clinicians and researchers who contributed to patient care and who helped to collect data at the Union Hospital, Tongji Medical College, Huazhong University of Science and Technology. And data are available upon reasonable request.

Funding: None.

Conflict of Interest: The authors have no conflicts of interest to disclose.

References

1. Kim SW, Song SH, Lee HS, Noh WJ, Oak C, Ahn YC, Lee KD. Intraoperative Real-Time Localization of Normal Parathyroid Glands With Autofluorescence Imaging. J Clin Endocrinol Metab. 2016; 101:4646-4652.
2. Bilezikian JP, Khan A, Potts JT Jr, *et al*. Hypoparathyroidism in the adult: Epidemiology, diagnosis, pathophysiology, target-organ involvement, treatment, and challenges for future research. J Bone Miner Res. 2011; 26:2317-2337.
3. Shoback D. Clinical practice. Hypoparathyroidism. N Engl J Med. 2008; 359:391-403.
4. Kose E, Rudin AV, Kahramangil B, Moore E, Aydin H, Donmez M, Krishnamurthy V, Siperstein A, Berber E. Autofluorescence imaging of parathyroid glands: An assessment of potential indications. Surgery. 2020; 167:173-179.
5. Tufano RP, Clayman G, Heller KS, Inabnet WB, Kebebew

E, Shaha A, Steward DL, Tuttle RM; American Thyroid Association Surgical Affairs Committee Writing Task Force. Management of recurrent/persistent nodal disease in patients with differentiated thyroid cancer: a critical review of the risks and benefits of surgical intervention versus active surveillance. Thyroid. 2015; 25:15-27.
6. Papavramidis TS, Chorti A, Tzikos G, Anagnostis P, Pantelidis P, Pliakos I, Panidis S, Papaioannou M, Bakkar S, Unal E, Michalopoulos A. The effect of intraoperative autofluorescence monitoring on unintentional parathyroid gland excision rates and postoperative PTH concentrations-a single-blind randomized-controlled trial. Endocrine. 2021; 72:546-552.
7. Kim Y, Kim SW, Lee KD, Ahn YC. Real-time localization of the parathyroid gland in surgical field using Raspberry Pi during thyroidectomy: a preliminary report. Biomed Opt Express. 2018; 9:3391-3398.
8. Berber E, Akbulut S. Can near-infrared autofluorescence imaging be used for intraoperative confirmation of parathyroid tissue? J Surg Oncol. 2021; 124:1008-1013.
9. van den Bos J, van Kooten L, Engelen SME, Lubbers T, Stassen LPS, Bouvy ND. Feasibility of indocyanine green fluorescence imaging for intraoperative identification of parathyroid glands during thyroid surgery. Head Neck. 2019; 41:340-348.
10. Patel HP, Chadwick DR, Harrison BJ, Balasubramanian SP. Systematic review of intravenous methylene blue in parathyroid surgery. Br J Surg. 2012; 99:1345-1351.
11. Paras C, Keller M, White L, Phay J, Mahadevan-Jansen A. Near-infrared autofluorescence for the detection of parathyroid glands. J Biomed Opt. 2011; 16:067012.
12. Shi C, Tian B, Li S, Shi T, Qin H, Liu S. Enhanced identification and functional protective role of carbon nanoparticles on parathyroid in thyroid cancer surgery: A retrospective Chinese population study. Medicine (Baltimore). 2016; 95:e5148.
13. Biello A, Kinberg EC, Wirtz ED. Thyroidectomy. StatPearls. Treasure Island (FL): StatPearls Publishing Copyright© 2021, StatPearls Publishing LLC.; 2021.
14. Papavramidis TS, Pliakos I, Chorti A, Panidis S, Kotsovolis G, Stelmach V, Koutsoumparis D, Bakkar S, Michalopoulos A. Comparing Ligasure™ Exact dissector with other energy devices in total thyroidectomy: a pilot study. Gland Surg. 2020; 9:271-277.
15. Kazaure HS, Zambeli-Ljepovic A, Oyekunle T, Roman SA, Sosa JA, Stang MT, Scheri RP. Severe Hypocalcemia After Thyroidectomy: An Analysis of 7366 Patients. Ann Surg. 2021; 274:e1014-e1021.
16. Rudin AV, McKenzie TJ, Thompson GB, Farley DR, Lyden ML. Evaluation of Parathyroid Glands with Indocyanine Green Fluorescence Angiography After Thyroidectomy. World J Surg. 2019; 43:1538-1543.
17. Hall NC, Plews RL, Agrawal A, Povoski SP, Wright CL, Zhang J, Martin EW Jr, Phay J. Intraoperative scintigraphy using a large field-of-view portable gamma camera for primary hyperparathyroidism: initial experience. Biomed Res Int. 2015; 2015:930575.
18. Wang B, Du ZP, Qiu NC, Liu ME, Liu S, Jiang DZ, Zhang W, Qiu M. Application of carbon nanoparticles accelerates the rapid recovery of parathyroid function during thyroid carcinoma surgery with central lymph node dissection: A retrospective cohort study. Int J Surg. 2016; 36:164-169.
19. Farrag T, Weinberger P, Seybt M, Terris DJ. Point-of-care rapid intraoperative parathyroid hormone assay of needle aspirates from parathyroid tissue: A substitute for frozen sections. Am J Otolaryngol. 2011; 32:574-577.
20. Kikumori T, Inaishi T, Miyajima N, Shibata M, Takeuchi D. Robust, quick, and convenient intraoperative method to differentiate parathyroid tissue. Surgery. 2020; 167:385-389.
21. Abbaci M, De Leeuw F, Breuskin I, Casiraghi O, Lakhdar AB, Ghanem W, Laplace-Builhé C, Hartl D. Parathyroid gland management using optical technologies during thyroidectomy or parathyroidectomy: A systematic review. Oral Oncol. 2018; 87:186-196.
22. Kim SW, Lee HS, Lee KD. Intraoperative real-time localization of parathyroid gland with near infrared fluorescence imaging. Gland Surg. 2017; 6:516-524.
23. McWade MA, Sanders ME, Broome JT, Solórzano CC, Mahadevan-Jansen A. Establishing the clinical utility of autofluorescence spectroscopy for parathyroid detection. Surgery. 2016; 159:193-202.
24. Squires MH, Shirley LA, Shen C, Jarvis R, Phay JE. Intraoperative Autofluorescence Parathyroid Identification in Patients With Multiple Endocrine Neoplasia Type 1. JAMA Otolaryngol Head Neck Surg. 2019; 145:897-902.
25. Ladurner R, Sommerey S, Arabi NA, Hallfeldt KKJ, Stepp H, Gallwas JKS. Intraoperative near-infrared autofluorescence imaging of parathyroid glands. Surg Endosc. 2017; 31:3140-3145.
26. Benmiloud F, Rebaudet S, Varoquaux A, Penaranda G, Bannier M, Denizot A. Impact of autofluorescence-based identification of parathyroids during total thyroidectomy on postoperative hypocalcemia: a before and after controlled study. Surgery. 2018; 163:23-30.
27. Takahashi T, Yamazaki K, Ota H, Shodo R, Ueki Y, Horii A. Near-Infrared Fluorescence Imaging in the Identification of Parathyroid Glands in Thyroidectomy. Laryngoscope. 2021; 131:1188-1193.
28. Benmiloud F, Godiris-Petit G, Gras R, Gillot JC, Turrin N, Penaranda G, Noullet S, Chéreau N, Gaudart J, Chiche L, Rebaudet S. Association of Autofluorescence-Based Detection of the Parathyroid Glands During Total Thyroidectomy With Postoperative Hypocalcemia Risk: Results of the PARAFLUO Multicenter Randomized Clinical Trial. JAMA Surg. 2020; 155:106-112.
29. McWade MA, Paras C, White LM, Phay JE, Solórzano CC, Broome JT, Mahadevan-Jansen A. Label-free intraoperative parathyroid localization with near-infrared autofluorescence imaging. J Clin Endocrinol Metab. 2014; 99:4574-4580.
30. Squires MH, Jarvis R, Shirley LA, Phay JE. Intraoperative Parathyroid Autofluorescence Detection in Patients with Primary Hyperparathyroidism. Ann Surg Oncol. 2019; 26:1142-1148.

Received June 9, 2022; Revised June 25, 2022; Accepted June 27, 2022.

§These authors contributed equally to this work.
*Address correspondence to:
Wei Shi and Shoupeng Zhang, Department of Thyroid and Breast Surgery, Union Hospital, Tongji Medical College, Huazhong University of Science and Technology, 1277 Jiefang Avenue, Wuhan 430022, Hubei, China.
E-mail: shiweihust@163.com, 2013xh0903@hust.edu.cn

Released online in J-STAGE as advance publication June 29, 2022.